Hindawi
Shock and Vibration
Volume 2020, Article ID 8839761, 11 pages
https://doi.org/10.1155/2020/8839761

Research Article

Experimental Investigation on the Energy Storage Characteristics of Red Sandstone in Triaxial Compression Tests with Constant Confining Pressure

Liuliu Li[1] **and Fengqiang Gong**[1,2]

[1]*School of Resources and Safety Engineering, Central South University, Changsha 410083, China*
[2]*School of Civil Engineering, Southeast University, Nanjing 211189, China*

Correspondence should be addressed to Fengqiang Gong; fengqiangg@126.com

Received 27 September 2020; Revised 31 October 2020; Accepted 2 November 2020; Published 25 November 2020

Academic Editor: Guangchao Zhang

The elastic energy stored in deep rock in three-dimensional stress environment is the energy source of rockburst. To investigate the energy storage characteristics of deep rock under different confining pressures, a series of triaxial single-cyclic loading-unloading compression tests were conducted on red sandstone specimens under eight confining pressures. The input energy density, elastic energy density, and dissipative energy density of the specimen in axial, circumferential, and total directions can be obtained by the area diagram integration method. The results show that the input energy density in the axial direction accounts for the largest logarithmic proportion of the total input energy density, and the relationship between all energy density parameters and unloading level can be described by quadratic function. In the axial direction, there is a linear function relationship among elastic energy density, dissipative energy density, and input energy density. In the circumferential direction, there is a quadratic function relationship among elastic energy density, dissipative energy density, and input energy density. For the total energy density parameters of the rock specimen, the relationship among elastic energy density, dissipative energy density, and input energy density conforms to the quadratic function. According to the above correlation function, the elastic energy stored in deep rock under different confining pressures can be accurately obtained, which provides a foundation for studying the mechanism of rockburst under three-dimensional unloading from the energy perspective.

1. Introduction

With the development of deep engineering, more and more rockburst disasters are encountered in the process of deep rock excavation [1–6]. Rockburst is a kind of disaster caused by the violent release of elastic energy stored in deep rocks [4–11], and the elastic energy accumulated in deep rock under high confining pressure is the energy source of rockburst. Many researchers have analysed and predicted rockburst from the perspective of energy [4, 10–16]. It is a basic problem of rockburst research to accurately evaluate or calculate the elastic energy of deep rocks under high stress in one or three dimensions [17, 18]. Energy conversion is an essential characteristic of material physical processes, which runs through all stages of rock or rock mass deformation [19–21]. The energy storage, dissipation, and release during the rock deformation process are closely related to the damage state [19, 22–32]. Therefore, it is necessary to study the internal mechanism of rock deformation from the perspective of energy storage and dissipation. To date, a great number of attempts related to the energy conversion of rock materials have been carried out and some valuable achievements have been achieved. Considering the uniaxial compression tests, Li et al. [24] presented that the prepeak absorbed strain energy, damage strain energy, and elastic strain energy all increased with the increase of strain rate. On the basis of uniaxial cyclic loading-unloading compressive tests, Meng et al. [30, 31] investigated the characteristics of energy accumulation and dissipation during rock deformation and implied that with the increase of axial load stress,

the total absorbed energy density increased the fastest, followed by the elastic energy density, and the dissipative energy density increased the slowest. Gong et al. [18, 25], Luo and Gong [26, 27], and Yang et al. [28] researched the characteristic of energy storage and dissipation in the process of rock deformation and found that there are strong linear relationships among elastic energy, dissipative energy, and total input energy. Based on the triaxial compression tests, Huang and Li [17] found that the initial confining pressure had a significant influence on the prepeak conversion rate of dissipative energy and elastic energy. Zhang and Gao [33] studied the energy evolution of red sandstone under different confining pressures and found that with the increase of confining pressure, the energy storage limit of rock increased in the form of power index.

Although the energy analysis method has been widely applied to the field of rock deformation mechanism and engineering owing to the superiority of making up the shortcomings of classical elastoplastic mechanics theory [31–35], there are few studies which focus on the relationships of elastic energy density, dissipative energy density, and input energy density under triaxial compression in the aforementioned works. It is necessary to study the energy storage and dissipation in the process of rock deformation.

In this paper, a series of triaxial single-cyclic loading-unloading compression tests were conducted on red sandstone specimens under eight confining pressures. The area graph integration method and stress-strain curve were combined to calculate three kinds of energy density parameters (the elastic energy density, dissipative energy density, and input energy density), and the relationships among these three energy density parameters under different axial or confining pressures in different directions were investigated. The energy storage and dissipation characteristics of red sandstone under triaxial compression were also analysed. The research results help us to further understand the energy storage and dissipation characteristics in triaxial compression tests with constant confining pressure.

2. Experimental Study and Methods

2.1. Specimen Preparation and Test Equipment. Red sandstone, which is from the city of Linyi in the Shandong Province, was chosen for laboratory experiments. Cylindrical specimens obtained by drilling core were used in this experiment. The diameter (D) and height (H) of the specimens were 50 mm and 100 mm, respectively. All rock specimens used for testing are integrated without cracks and have good homogeneity. To reduce the experimental error, the sides and end faces of all rock specimens were polished smoothly. Meanwhile, the upper and lower end faces of all rock specimens were parallel to meet the standards of the International Society for Rock Mechanics (ISRM) standard [35].

These experiments were carried out by MTS 815 electrohydraulic servo rock mechanics testing machine (Figure 1). The testing machine consists of loading rack, servo system control box, hydraulic pump, triaxial pressure chamber, and data display screen. In the tests, the axial and circumferential forces of rock specimens were obtained by pressure sensors. Meanwhile, the axial and circumferential strains of rock specimens were measured by the axial and circumferential extensometers, respectively.

2.2. Test Scheme. To study the energy storage and dissipation characteristics of red sandstone under triaxial compression, triaxial single-cyclic loading-unloading compression (TSCLUC) experiments under eight presupposed confining pressures (5, 10, 15, 20, 30, 40, 50, and 60 MPa) were conducted. Considering that the loading-unloading paths under each confining pressure are the same, the first experiment, whose confining pressure was 5 MPa, was used to elaborate the experimental procedures. The detailed procedures can be shown in Figure 2.

Firstly, the forces of axial and circumferential directions were applied on the red sandstone specimen at the rate of 0.1 MPa/s simultaneously and the force was stopped when the confining pressure reached the preset value of 5 MPa. Meanwhile, preset confining pressure value is regarded as unloading point. Then, all the forces applied to the specimen were decreased to zero at the rate of 0.1 MPa/s. Finally, keeping the rock specimen at the confining pressure of 5 MPa, displacement control was adopted to load on the rock specimen at the rate of 0.1 mm/min in the axial direction until peak strength. For the other seven experiments, the loading-unloading method was the same as the first experiment.

2.3. Energy Calculation Method of Three Energy Parameters. According to the first law of thermodynamics, the total input energy density, elastic energy density, and dissipation energy density of rock materials in the process of stress and deformation satisfy the following relation [36]:

$$U = U_e + U_d, \tag{1}$$

where U is the total input energy density produced by the work of external force, U_d is the dissipative energy density and used for the internal damage and plastic deformation of rock unit, and U_e is the elastic energy density stored in rock unit during the loading-unloading process, which is formed in the stage of elastic strain of rock unit. After the external force is removed, this part energy of rock can be recovered.

In conventional triaxial compression tests, the stress state changes to biaxial compression; that is, $\sigma_2 = \sigma_3$. At this time, the strain energy density absorbed by rock elements can be expressed as

$$U = \int \sigma_1 \, d\varepsilon_1 + 2 \int \sigma_3 \, d\varepsilon_3. \tag{2}$$

Equation (2) can be interpreted as that the total work of external force on rock element can be divided into axial and circumferential parts in conventional triaxial tests.

To eliminate the influence of individual differences of rock specimens on the experiment, energy density was adopted for all three kinds of energy. The interrelation among the three energy density parameters can be expressed as

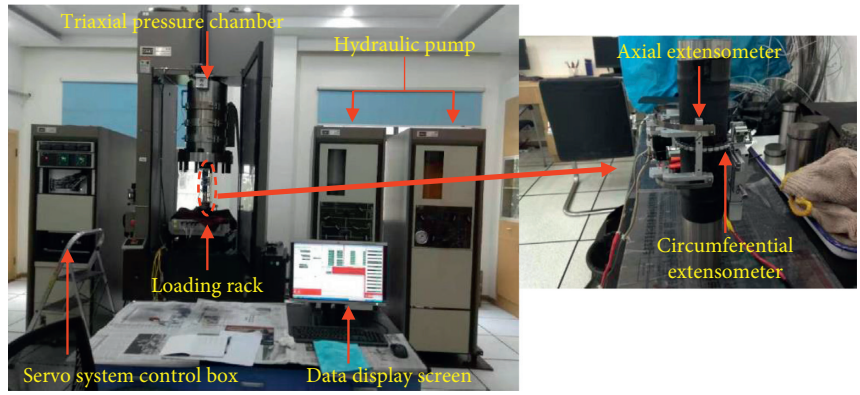

Figure 1: MTS 815 experimental system.

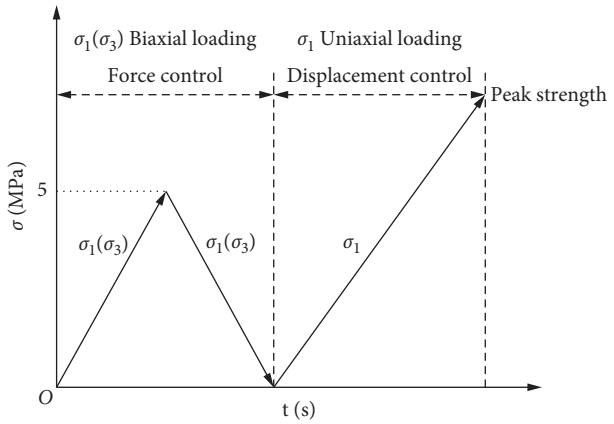

Figure 2: Diagram of triaxial loading-unloading segment.

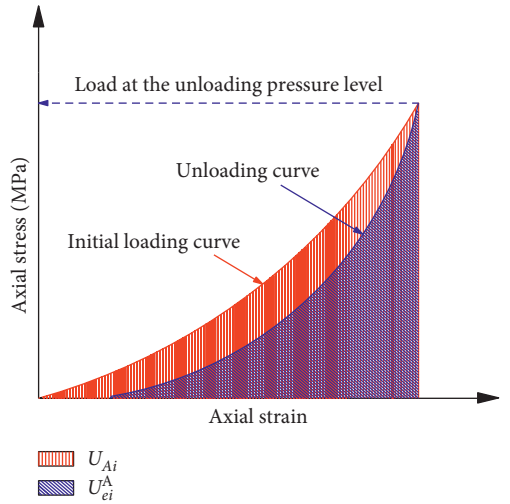

Figure 3: Schematic diagram energy density parameters in the axial direction.

$$\begin{aligned} U_i &= U_{ei} + U_{di}, \\ U_i &= U_{Ai} + U_{Ci}, \\ U_{Ai} &= U_{ei}^{A} + U_{di}^{A}, \\ U_{Ci} &= U_{ei}^{C} + U_{di}^{C}, \end{aligned} \tag{3}$$

where U_i, U_{ei}, and U_{di} are the total input energy density (TIED), total elastic energy density (TEED), and total dissipative energy density (TDED), respectively. U_{Ai}, U_{ei}^{A}, and U_{di}^{A} are the axial input energy density (AIED), axial elastic energy density (AEED), and axial dissipative energy density (ADED), respectively. U_{Ci}, U_{ei}^{C}, and U_{di}^{C} are the circumferential input energy density (CIED), circumferential elastic energy density (CEED), and circumferential dissipative energy density (CDED), respectively. i is the axial or confining pressure level.

Three kinds of energy density parameters can be obtained by area graph integration. The schematic diagram of energy density parameters was shown in Figure 3. The calculation method of circumferential energy density parameters is the same as that of axial energy density parameters. Therefore, taking the axial direction as an example, the value of AIED was determined by the area between the initial loading curve and the strain axis. The value of AEED was determined by the area between the unloading curve and the strain axis. Hence, the value of ADED at the unloading pressure level was obtained by the difference between the AIED and the corresponding AEED.

3. Stress-Strain Curves of Rock Specimens

Under the action of external force, rock will undergo continuous deformation and even failure when the forces reach the failure strength of rock specimen. In this process, the force and deformation of the rock can be detected by the sensors of the test system. Figure 4 shows the stress-strain curves of red sandstone under eight confining pressures. The deformation process of red sandstone can be divided into two stages: initial compaction stage and elastic deformation stage. In the initial compaction stage, the microcracks and pores in the rock were compacted under the action of external force. At this stage, the rock hardly deformed after the external force was removed. In the elastic deformation stage, the microcracks in the rock began to develop. The deformation in the elastic stage is generally recoverable. Because the rock is not an ideal elastic body, the residual deformation will occur after the external force is removed in the elastic stage. To compare the difference between the circumferential

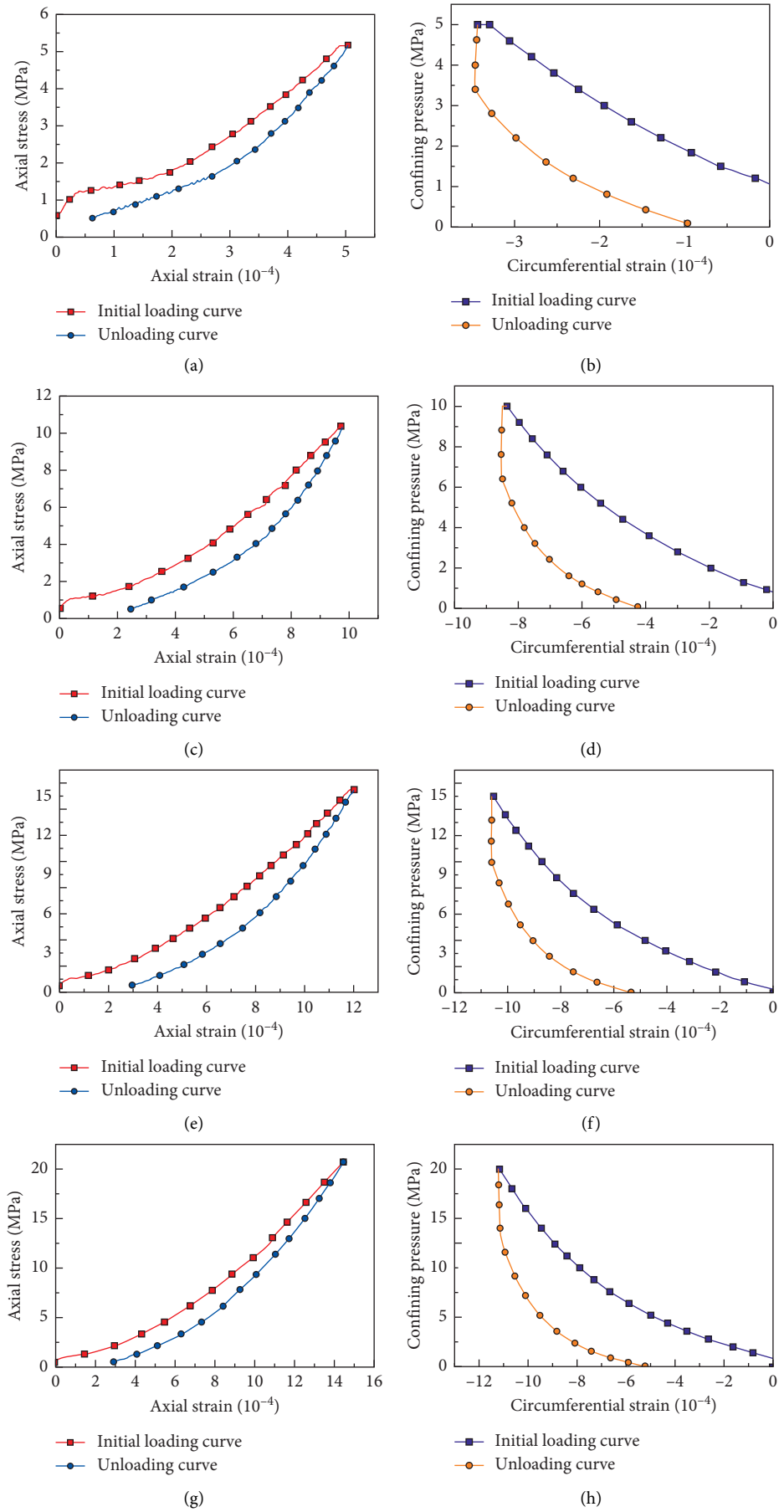

Figure 4: Continued.

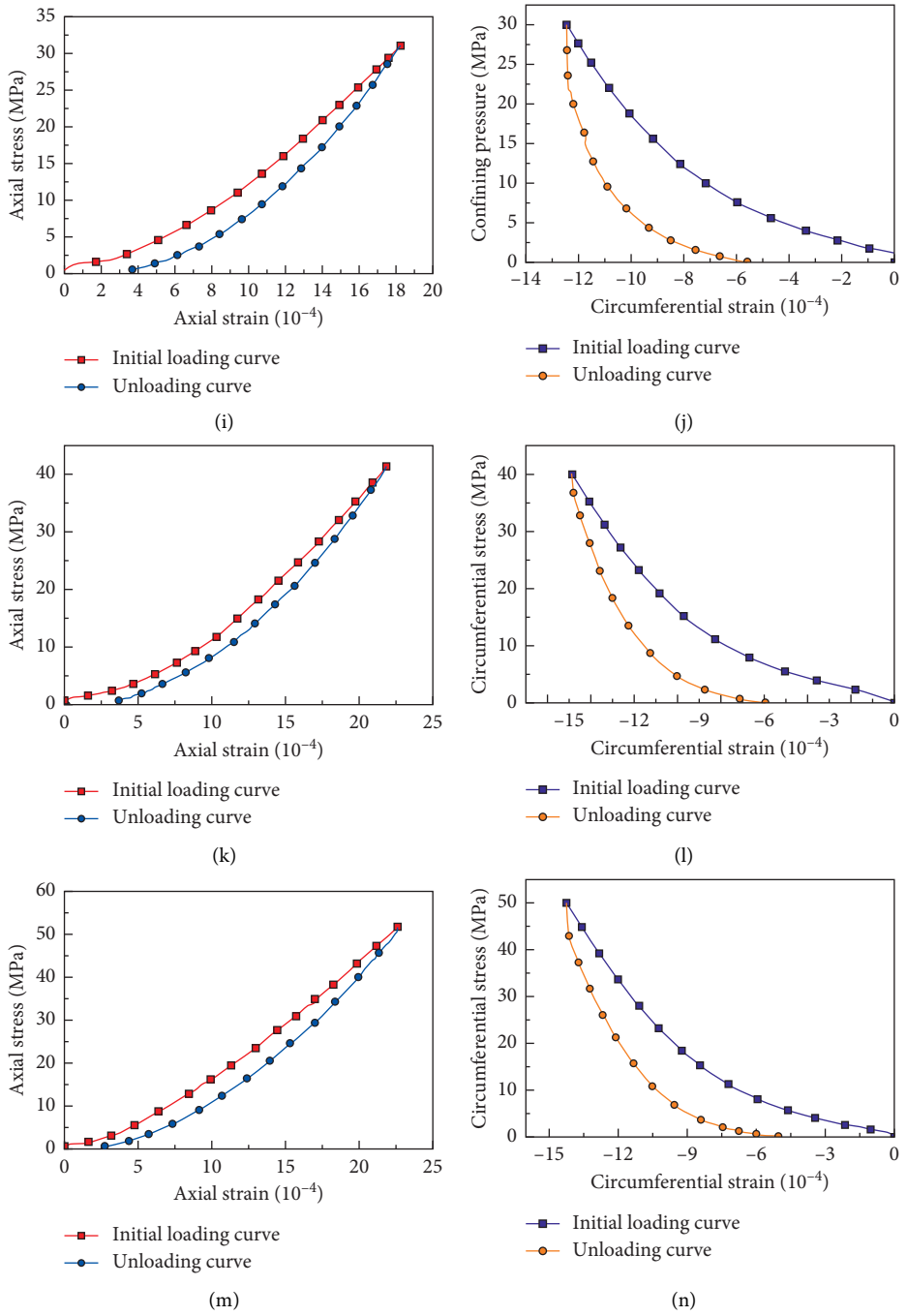

Figure 4: Continued.

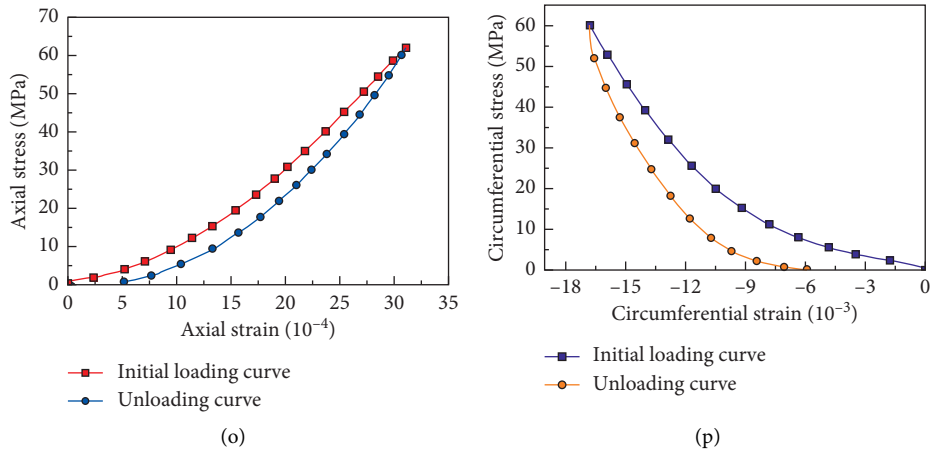

Figure 4: Stress-strain curves of eight confining pressures in TSCLUC tests. (a), (c), (e), (g), (i), (k), (m), and (o) axial loading-unloading curves and (b), (d), (f), (h), (j), (l), (n), and (p) circumferential loading-unloading curves. (a)$i_a = 5$ MPa, (b) $i_C = 5$ MPa, (c) $i_a = 10$ MPa, (d) $i_C = 10$ MPa, (e) $i_a = 15$ MPa, (f) $i_C = 15$ MPa, (g) $i_a = 20$ MPa, (h) $i_C = 20$ MPa, (i) $i_a = 30$ MPa, (j) $i_C = 30$ MPa, (k) $i_a = 40$ MPa, (l) $i_C = 40$ MPa, (m) $i_a = 50$ MPa, (n) $i_C = 50$ MPa, (o) $i_a = 60$ MPa, and (p) $i_C = 60$ MPa.

and axial stress-strain curves, the stress-strain curves under the confining pressure of 5 and 10 MPa were analysed. It can be found from Figures 4(a) and 4(c) that the area enclosed by the initial loading line and unloading line was little when the axial pressure is 5 and 10 MPa, which shows that there is little energy dissipation in the axial direction when axial pressure is little. However, as noted in Figures 4(b) and 4(d), at the same stress level, with the increase of confining pressure in the circumferential direction, the dissipative energy density becomes larger and larger, showing a different trend of energy change from the axial direction. The reason why this phenomenon appeared was that circumferential surface area is large and producing the same deformation needs more work. It can be seen from Figures 4(b), 4(d), 4(f), 4(h), 4(j), 4(l), 4(n), and 4(p) that as the confining pressure increases from 5 to 60 MPa, the dissipative energy density decreases more and more obviously. Meanwhile, it can be found from Figure 4(p) that the area of the unloading line and the strain axis representing the circumferential elastic energy density has exceeded the area of the initial loading line and unloading line representing the circumferential dissipative energy density, which means that in the circumferential direction, the energy dissipation is greater than the storage at the initial stage, and with the increase of confining pressure, the energy storage is greater than the dissipation.

4. Test Results

4.1. Energy Storage and Dissipation Characteristics of Red Sandstone in the Axial Direction. According to the stress-strain curves of red sandstone specimens, three energy density parameters in different directions under eight confining pressures were obtained by area diagram integration. The detailed parameters of the three energy densities are listed in Tables 1–3, respectively.

Figure 5 displays the variation curves of AIED, AEED, and ADED (the coordinate point (0, 0) was adopted to rectify the deviation in Figures 5–10). As presented in Figure 5, three kinds of energy density parameters increased with the increasing of axial pressure, and they all obeyed the quadratic function. The growth rate of AIED is greater than that of AEED, and the growth rate of AEED is greater than that of ADED, which manifests the fact that energy storage is greater than energy dissipation in axial direction. The growth curve of AEED is close to the curve of AIED and the curve of ADED is far from the curve of AIED, which indicates that with the increasing of axial pressure, energy storage is dominant in the axial direction. Figure 6 showed the relationship between AEED, ADED, and AIED. The AEED and ADED increased linearly with the AIED, whose correlation coefficients were 0.9989 and 0.9800, respectively. This linear relationship is consistent with that obtained by Sepehri et al. [14, 18, 25, 26, 37] in other types of experiments.

4.2. Energy Storage and Dissipation Characteristics of Red Sandstone in the Circumferential Direction. As shown in Figure 7, the variation curves of CIED, CEED, and CDED under eight confining pressures follow the quadratic function. Compared to the axial direction, the growth trend of CEED and CDED is different. Before the confining pressure of 50 MPa, the growth of the CDED is greater than that of the CEED. When the confining pressure is 50–60 MPa, the growth of the CEED is greater than that of the CDED. This shows that the confining pressure of 50 MPa is the turning point of the energy from dissipation to accumulation in circumferential direction. The reason why this phenomenon appeared was that the confining effect of circumferential force on rock deformation is less than the compression of axial force on rock when the confining pressure is less than 50 MPa. In this case, due to the axial compression, microcracks and pores in the rock develop rapidly in the circumferential direction, and the energy dissipation in the circumferential direction is greater than the energy storage.

Table 1: Three energy density parameters of red sandstone specimens in the axial direction.

Specimen ID	Axial pressure (MPa)	In the axial direction		
		AIED (mJ/mm^3)	AEED (mJ/mm^3)	ADED (mJ/mm^3)
S-T-1	5	0.0013	0.0010	0.0003
S-T-2	10	0.0042	0.0029	0.0013
S-T-3	15	0.0080	0.0055	0.0025
S-T-4	20	0.0118	0.0092	0.0026
S-T-5	30	0.0227	0.0174	0.0053
S-T-6	40	0.0345	0.0291	0.0054
S-T-7	50	0.0485	0.0394	0.0091
S-T-8	60	0.0735	0.0587	0.0148

Table 2: Three energy parameters of red sandstone specimens in the circumferential direction.

Specimen ID	Confining pressure (MPa)	In the circumferential direction		
		CIED (mJ/mm^3)	CEED (mJ/mm^3)	CDED (mJ/mm^3)
S-T-1	5	0.0020	0.0006	0.0014
S-T-2	10	0.0077	0.0018	0.0059
S-T-3	15	0.0118	0.0032	0.0086
S-T-4	20	0.0170	0.0047	0.0123
S-T-5	30	0.0268	0.0084	0.0184
S-T-6	40	0.0395	0.0178	0.0217
S-T-7	50	0.0464	0.0227	0.0237
S-T-8	60	0.0648	0.0363	0.0285

Table 3: Three energy parameters of red sandstone specimens in the total direction.

Specimen ID	Stress level (MPa)	In the total direction		
		TIED (mJ/mm^3)	TEED (mJ/mm^3)	TDED (mJ/mm^3)
S-T-1	5	0.0033	0.0016	0.0017
S-T-2	10	0.0118	0.0047	0.0071
S-T-3	15	0.0197	0.0086	0.0111
S-T-4	20	0.0286	0.0139	0.0147
S-T-5	30	0.0493	0.0258	0.0235
S-T-6	40	0.0734	0.0467	0.0267
S-T-7	50	0.0944	0.0622	0.0322
S-T-8	60	0.1375	0.0946	0.0429

However, with the increase of confining pressure, the confining effect of circumferential force on rock is greater than the compression of axial force on rock. The microcracks in the rock begin to close under the action of external force, and the storage of circumferential energy is gradually greater than the dissipation. Figure 8 implies the relationships between CEED, CDED, and CIED. The CEED and CDED increase exponentially with the CIED. Their correlation coefficients are more than 0.99, which has a very strong correlation. As noted in Figure 7, circumferential energy density variation characteristics show that the energy dissipation dominates in the circumferential direction when the confining pressure is less than 50 MPa.

4.3. Energy Storage and Dissipation Characteristics of Red Sandstone in the Total Direction. Similar to the characteristics of Figure 7, Figure 9 shows that the variation trend of three energy density parameters in the total direction. The TIED increased in the form of quadratic function with the increase of stress level, whose correlation coefficient is 0.9963. The TEED and TDED also obeyed the relationship and their correlation coefficients are 0.9968 and 0.9888, respectively. However, before the stress level is 20 MPa, the TDED is higher than the TEED. When the stress level is 20–60 MPa, the TDED is lower than the TEED. The reason why this phenomenon appeared is that the increase degree of the TDED is greater than that of the TEED before the stress level of 20 MPa. It can be found from Figure 10 that the quadratic function growth relationships of the TEED and TDED with the increasing of TIED in the total direction were found. The growth rate of TEED is higher than that of TDED, which demonstrates that the energy storage plays a dominant role in triaxial compression tests with constant confining pressure.

5. Discussion

Although rock is a kind of inhomogeneous material with joints and fissures, there is a certain regularity of energy transformation under triaxial compression. In the axial direction, there is a good linear relationship between the

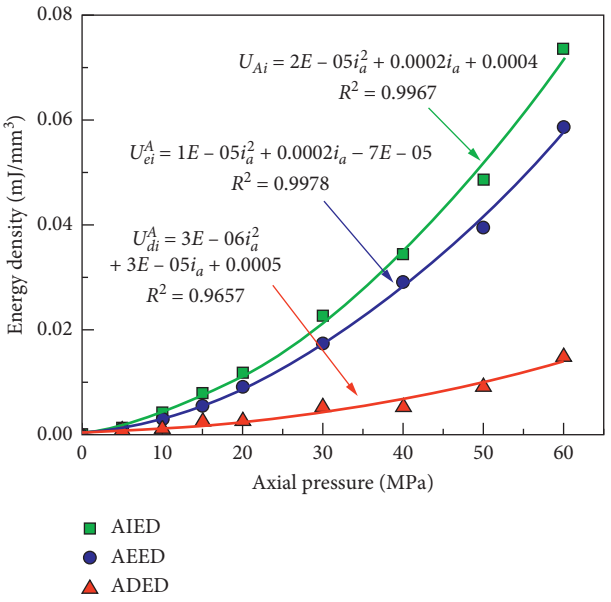

Figure 5: Variation curves of three energy density parameters under eight axial pressures.

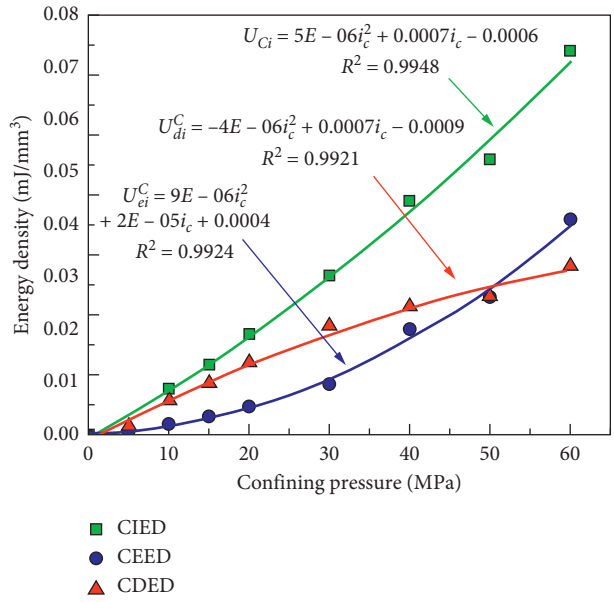

Figure 7: Variation curves of three energy density parameters under eight confining pressures.

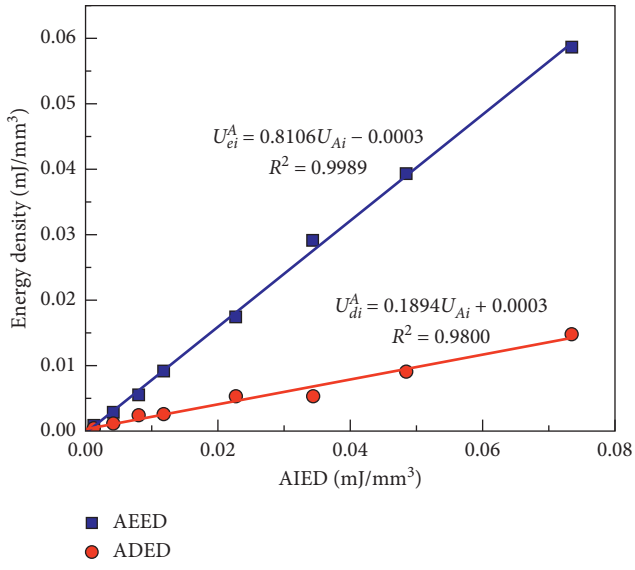

Figure 6: Relationships between AEED, ADED, and AIED.

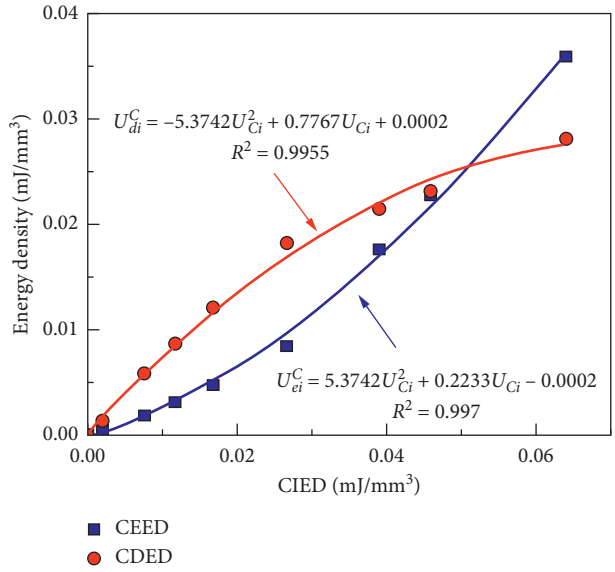

Figure 8: Relationships between CEED, CDED, and CIED.

AEED, ADED, and AIED, which is consistent with the findings of Gong et al. [18] under uniaxial compression. In the circumferential direction, there is a quadratic relationship between the CEED, CDED, and CIED. Due to the influence of circumferential energy transformation, TEED and TDED have a quadratic relationship with TIED, which provided a method for accurately estimating the energy parameters of deep rock under high confining pressure. Accurately obtaining the elastic energy of rock under three-dimensional high stress state is the basis and premise of evaluating rockburst intensity. According to the above correlation function, the elastic energy stored in deep rock under different confining pressures can be calculated accurately. On this basis, the three-dimensional high stress unloading test will be continued in the follow-up research. The intensity of rockburst can be accurately and quantitatively evaluated by analysing the energy released in the unloading process of high-energy-storage rock.

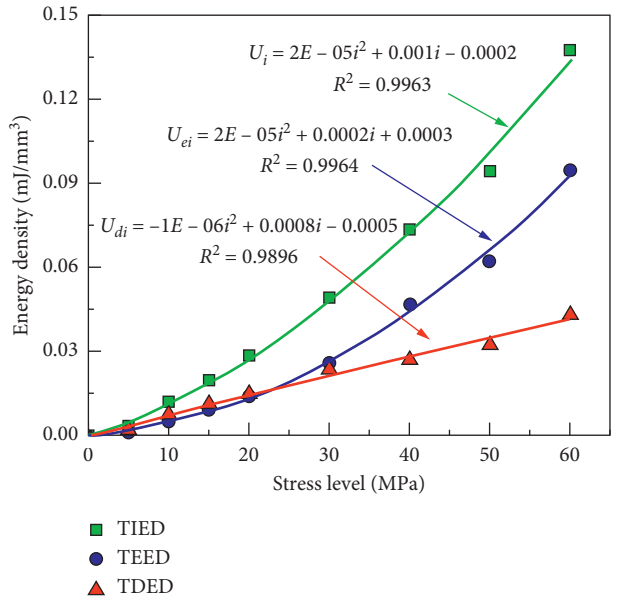

Figure 9: Variation curves of TIED, TEED, and TDED.

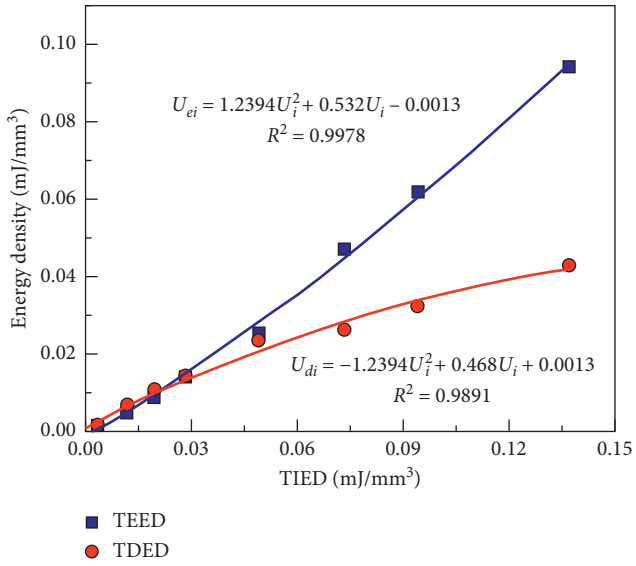

Figure 10: Relationships between TEED, TDED, and TIED.

6. Conclusions

A series of TSCLUC tests of red sandstone under eight confining pressures were conducted. The area graphic integration method was adopted to calculate the energy density parameters in different directions. The relationships of elastic energy density, dissipative energy density, and input energy density under different axial or confining pressures were analysed. The conclusions can be derived as follows.

(1) There is a strong linear relationship between the axial elastic energy density, the axial dissipative energy density, and the axial input energy density under triaxial compression. Energy storage dominates in the axial direction. With the increasing of axial pressure, the growth rate of axial input energy density is greater than that of axial elastic energy density, and the growth rate of axial elastic energy density is greater than that of axial dissipative energy density.

(2) Circumferential elastic energy density and circumferential dissipative energy density have a quadratic function relationship with circumferential input energy density under triaxial compression. When the confining pressure is less than 50 MPa, the growth rate of circumferential dissipative energy density is greater than that of circumferential elastic energy density. At this time, the energy dissipation is the main direction. When the confining pressure is between 50 and 60 MPa, the growth rate of the circumferential dissipative energy density is smaller than that of the circumferential elastic energy density.

(3) Similar to the circumferential direction, the relationship between the total elastic energy density and the total input energy density presents a quadratic function. By using the above relationship, the elastic energy stored in deep rock under three-dimensional stress environment can be accurately calculated as long as the total input energy is known, which provides a new method for accurately estimating the elastic energy of deep rock under different confining pressures. The above results provide a possibility to study the mechanism of rockburst induced by unloading of three-dimensional high-energy-storage rock from the perspective of energy.

Data Availability

All data generated or analysed during this study are included within this article.

Conflicts of Interest

The authors declare that there are no conflicts of interest regarding the publication of this paper.

Acknowledgments

This work was supported by the National Natural Science Foundation of China (Grant no. 41877272) and the Fundamental Research Funds for the Central Universities of Southeast University (Grant no. 2242020R10023).

References

[1] S. J. Li, X. T. Feng, Z. H. Li, B. R. Chen, C. Q. Zhang, and H. Zhou, "In situ monitoring of rockburst nucleation and evolution in the deeply buried tunnels of Jinping II hydropower station," *Engineering Geology*, vol. 137-138, pp. 85–96, 2012.

[2] F. Q. Gong, Y. L. Wang, and S. Luo, "Rockburst proneness criteria for rock materials: review and new insights," *Journal*

of Central South University, vol. 27, no. 10, pp. 2793–2821, 2020.

[3] X. B. Li, F. Q. Gong, M. Tao et al., "Failure mechanism and coupled static-dynamic loading theory in deep hard rock mining: a review," *Journal of Rock Mechanics and Geotechnical Engineering*, vol. 9, no. 4, pp. 767–782, 2017.

[4] Q. Jiang, X. T. Feng, T. B. Xiang, and G. S. Su, "Rockburst characteristics and numerical simulation based on a new energy index: a case study of a tunnel at 2,500 m depth," *Bulletin of Engineering Geology and the Environment*, vol. 69, no. 3, pp. 381–388, 2010.

[5] P. K. Kaiser and M. Cai, "Design of rock support system under rockburst condition," *Journal of Rock Mechanics and Geotechnical Engineering*, vol. 4, no. 3, pp. 215–227, 2012.

[6] F. Q. Gong, X. F. Si, X. B. Li, and S. Y. Wang, "Experimental investigation of strain rockburst in circular caverns under deep three-dimensional high-stress conditions," *Rock Mechanics and Rock Engineering*, vol. 52, no. 5, pp. 1459–1474, 2019.

[7] B. Y. Jiang, S. T. Gu, L. G. Wang, G. C. Zhang, and W. S. Li, "Strainburst process of marble in tunnel-excavation-induced stress path considering intermediate principal stress," *Journal of Central South University*, vol. 26, no. 4, pp. 984–999, 2019.

[8] F. Q. Gong, Y. Luo, X. B. Li, X. F. Si, and M. Tao, "Experimental simulation investigation on rockburst induced by spalling failure in deep circular tunnels," *Tunnelling and Underground Space Technology*, vol. 81, pp. 413–427, 2018.

[9] X. F. Si and F. Q. Gong, "Strength-weakening effect and shear-tension failure mode transformation mechanism of rockburst for fine-grained granite under triaxial unloading compression," *International Journal of Rock Mechanics and Mining Sciences*, vol. 131, Article ID 104347, 2020.

[10] S. Akdag, M. Karakus, G. D. Nguyen, and A. Taheri, "Strain burst vulnerability criterion based on energy-release rate," *Engineering Fracture Mechanics*, vol. 237, Article ID 107232, 2020.

[11] J. A. Wang and H. D. Park, "Comprehensive prediction of rockburst based on analysis of strain energy in rocks," *Tunnelling and Underground Space Technology*, vol. 16, no. 1, pp. 49–57, 2001.

[12] F. Q. Gong, J. Y. Yan, X. B. Li, and S. Luo, "A peak-strength strain energy storage index for rock burst proneness of rock materials," *International Journal of Rock Mechanics and Mining Sciences*, vol. 117, pp. 76–89, 2019.

[13] S. Akdag, M. Karakus, G. D. Nguyen, A. Taheri, and T. Bruning, "Evaluation of the propensity of strain burst in brittle granite based on post-peak energy analysis," *Underground Space*, 2019.

[14] M. Sepehri, D. B. Apel, S. Adeeb, P. Leveille, and R. A. Hall, "Evaluation of mining-induced energy and rockburst prediction at a diamond mine in Canada using a full 3*D* elastoplastic finite element model," *Engineering Geology*, vol. 266, Article ID 105457, 2019.

[15] H. M. Tian, W. Z. Chen, C. S. Ma, D. S. Yang, and X. J. Tan, "Energy release analysis of a severe rockburst in a headrace tunnel crossing a tectonic stress zone," *Shock and Vibration*, vol. 2019, no. 2, 9 pages, Article ID 8959845, 2019.

[16] L. Chen and L. J. Guo, "Discussions on the complete strain energy characteristics of deep granite and assessment of rockburst tendency," *Shock and Vibration*, vol. 2020, no. 7, 9 pages, Article ID 8825505, 2020.

[17] D. Huang and Y. R. Li, "Conversion of strain energy in triaxial unloading tests on marble," *International Journal of Rock Mechanics and Mining Sciences*, vol. 66, pp. 160–168, 2014.

[18] F. Q. Gong, J. Y. Yan, S. Luo, and X. B. Li, "Investigation on the linear energy storage and dissipation laws of rock materials under uniaxial compression," *Rock Mechanics and Rock Engineering*, vol. 52, no. 11, pp. 4237–4255, 2019.

[19] H. P. Xie, L. Y. Li, R. D. Peng, and Y. Ju, "Energy analysis and criteria for structural failure of rocks," *Journal of Rock Mechanics and Geotechnical Engineering*, vol. 1, no. 1, pp. 11–20, 2009.

[20] M. W. Zhang, Q. B. Meng, and S. D. Liu, "Energy evolution characteristics and distribution laws of rock materials under triaxial cyclic loading and unloading compression," *Advances in Materials Science and Engineering*, vol. 2017, Article ID 5471571, 16 pages, 2017.

[21] G. C. Zhang, F. L. He, H. G. Jia, and Y. H. Lai, "Analysis of gateroad stability in relation to yield pillar size: a case study," *Rock Mechanics and Rock Engineering*, vol. 50, no. 5, pp. 1263–1278, 2017.

[22] R. D. Peng, Y. Ju, J. G. Wang, H. P. Xie, F. Gao, and L. T. Mao, "Energy dissipation and release during coal failure under conventional triaxial compression," *Rock Mechanics and Rock Engineering*, vol. 48, no. 2, pp. 509–526, 2015.

[23] T. Kanaya and G. Hirth, "Brittle to semibrittle transition in quartz sandstone: energetics," *Journal of Geophysical Research: Solid Earth*, vol. 123, no. 1, pp. 84–106, 2018.

[24] Y. R. Li, D. Huang, and X. A. Li, "Strain rate dependency of coarse crystal marble under uniaxial compression: strength, deformation and strain energy," *Rock Mechanics and Rock Engineering*, vol. 47, no. 4, pp. 1153–1164, 2014.

[25] F. Q. Gong, S. Luo, and J. Y. Yan, "Energy storage and dissipation evolution process and characteristics of marble in three tension-type failure tests," *Rock Mechanics and Rock Engineering*, vol. 51, no. 11, pp. 3613–3624, 2018.

[26] S. Luo and F. Q. Gong, "Linear energy storage and dissipation laws during rock fracture under three-point flexural loading," *Engineering Fracture Mechanics*, vol. 234, Article ID 107102, 2020.

[27] S. Luo and F. Q. Gong, "Linear energy storage and dissipation laws of rocks under preset angle shear conditions," *Rock Mechanics and Rock Engineering*, vol. 53, no. 7, pp. 3303–3323, 2020.

[28] J. J. Yang, F. Q. Gong, D. Q. Liu, and Z. X. Liu, "Experimental study on the influence of specimen shape on rockburst proneness of red sandstone," *Shock and Vibration*, vol. 2020, no. 9, 17 pages, Article ID 4182861, 2020.

[29] M. M. He, F. Pang, H. T. Wang, J. W. Zhu, and Y. S. Chen, "Energy dissipation-based method for strength determination of rock under uniaxial compression," *Shock and Vibration*, vol. 2020, Article ID 8865958, 13 pages, 2020.

[30] Q. B. Meng, M. W. Zhang, L. J. Han, H. Pu, and T. Y. Nie, "Effects of acoustic emission and energy evolution of rock specimens under the uniaxial cyclic loading and unloading compression," *Rock Mechanics and Rock Engineering*, vol. 49, no. 10, pp. 3873–3886, 2016.

[31] Q. B. Meng, M. W. Zhang, Z. Z. Zhang, L. J. Han, and H. Pu, "Experimental research on rock energy evolution under uniaxial cyclic loading and unloading compression," *Geotechnical Testing Journal*, vol. 41, no. 4, pp. 717–729, 2018.

[32] X. X. Liu, Y. Li, F. J. Zhao, Y. M. Zhou, W. W. Wang, and S. N. Li, "Experimental research on mechanical and energy characteristics of reinforced rock under dynamic loading," *Shock and Vibration*, vol. 2019, no. 2, 11 pages, Article ID 4356729, 2019.

[33] Z. Z. Zhang and F. Gao, "Confining pressure effect on rock energy," *Chinese Journal of Rock Mechanics and Engineering*, vol. 34, no. 1, pp. 1–11, 2015.

[34] P. L. P. Wasantha, P. G. Ranjith, and S. S. Shao, "Energy monitoring and analysis during deformation of bedded-sandstone: use of acoustic emission," *Ultrasonics*, vol. 54, no. 1, pp. 217–226, 2014.

[35] C. E. Fairhurst and J. A. Hudson, "Draft ISRM suggested method for the complete stress-strain curve for intact rock in uniaxial compression," *International Journal of Rock Mechanics and Mining Sciences*, vol. 36, no. 3, pp. 281–289, 1999.

[36] H. P. Xie, R. D. Peng, and Y. Ju, "Energy dissipation of rock deformation and fracture," *Chinese Journal of Rock Mechanics and Engineering*, vol. 23, no. 21, pp. 3565–3570, 2004.

[37] F. Q. Gong and J. Hu, "Energy dissipation characteristic of red sandstone in the dynamic brazilian disc test with SHPB setup," *Advances in Civil Engineering*, vol. 2020, Article ID 7160937, 10 pages, 2020.